Nematic order in the vicinity of a vortex in superconducting FeSe

Debanjan Chowdhury, Erez Berg, and Subir Sachdev

Department of Physics, Harvard University, Cambridge Massachusetts 02138, USA

We present a phenomenological theory of the interplay between nematic order and superconductivity in the vicinity of a vortex induced by an applied magnetic field. Nematic order can be strongly enhanced in the vortex core. As a result, the vortex cores become elliptical in shape. For the case where there is weak bulk nematic order at zero magnetic field, the field-induced eccentricity of the vortex core has a slow power-law decay away from the core. Conversely, if the nematic order is field induced, then the eccentricity is confined to the vortex core. We discuss the relevance of our results to recent scanning tunneling microscopy experiments on FeSe [Song *et al.*, Science **332**, 1410 (2011)].

PACS number(s): 74.70.Xa, 74.20.De, 74.25.Uv

I. INTRODUCTION

The unconventional superconductors have a rich phase diagram determined by the interplay of multiple competing, or coexisting, types of order. Nematic order (which breaks the C_4 symmetry of the underlying square lattice down to C_2) has been shown to emerge in certain regimes of the phase diagrams of the copper-oxide[1–6] and the iron-based[7–13] superconductors. In the latter case, the nematic order accompanies (and, in some cases, precedes) the magnetic order that occurs at a wave vector that breaks the lattice rotational symmetry.

Recently, the structure of the vortex cores in the mixed state of clean FeSe films was studied by means of scanning tunneling microscopy (STM).[14] Strong anisotropy was observed in the zero bias conductance map around the cores, which have an eccentricity of the order of unity. Although the lattice structure of FeSe at low temperature is orthorhombic,[15] it has been claimed[14] that the crystalline anisotropy (of the order of a few tenths of a precent) is too small to explain the large anisotropy of the vortex cores, which is likely to have an electronic origin.

This experiment raises several questions, some of which we address in this article: Assuming there is an electronic nematic order in superconducting FeSe, what is its microscopic origin? What is its relation to superconductivity (e.g., are these two types of order competing)? Is the nematic order localized in the vortex cores (and, hence, stabilized by the application of the magnetic field), or does it extend throughout the system (and is it apparent only in the STM spectrum near the cores)?

Here, we study the structure of the vortex core using a phenomenological Landau-Ginzburg (LG) theory in terms of two competing order parameters. Using our LG analysis we have calculated the structure of an isolated vortex in the presence of the nematic order. Our main result is that by looking at the profile of the gap near the vortex core, it is possible to distinguish between two different configurations of the nematic order, namely the presence of a localized nematic order within the superconducting vortex as opposed to the presence of a long range nematic order in the system. If the nematic order is localized at the core, the superconducting gap should be anisotropic only near the core and the anisotropy decays exponentially as we move away from the core. On the other hand, if the nematic order is long ranged, the superconducting gap should exhibit an anisotropy that decays as a power law. If the nematic order is near its critical point,

there is a large region in which the anisotropy of the gap depends logarithmically on the distance, eventually crossing over to a power law. Moreover, we find qualitative differences in the shape of the contours of constant gap around the core in the different cases. If the nematic order exists only in the cores, the equal-gap contours tend to be elliptical; if the nematic order is long ranged, we find that the gap function tends to develop a "four-lobe" structure, with more pronounced higher harmonics. These features can be sought in STM experiments by mapping the magnitude of the gap around the core as a function of position.

The article is organized as follows: In Sec. II we introduce the LG functional with the two competing order parameters and carry out a preliminary analysis in the absence of the anisotropy. In Sec. III, we investigate the mean-field phase diagram of a single vortex. In Sec. IV, we introduce the anisotropy and perform a numerical minimization of the functional, commenting on the interesting features. Finally, in Sec. V, we present our analytical results explaining the various interesting features observed by minimizing the free energy.

II. MODEL

We consider an LG-type free energy for two competing order parameters: a complex field Ψ, describing the superconducting order parameter, and a real field ϕ, which describes a nematic order that competes with the superconducting order parameter. The form of the free energy density is given by

$$\mathcal{F} = \mathcal{F}_s + \mathcal{F}_\phi + \mathcal{F}_a + \frac{\gamma}{2}|\Psi|^2\phi^2, \qquad (1)$$

$$\mathcal{F}_s = \frac{\kappa_\psi}{2}|(-i\nabla - e^*\mathbf{A})\Psi|^2 - \frac{\psi_0^2}{2}|\Psi|^2 + \frac{1}{4}|\Psi|^4, \quad (2)$$

$$\mathcal{F}_\phi = \frac{\kappa_\phi}{2}(\nabla\phi)^2 - \frac{\phi_0^2}{2}\phi^2 + \frac{1}{4}\phi^4, \qquad (3)$$

$$\mathcal{F}_a = \frac{\lambda_1}{2}\phi[|(-i\partial_x - e^*A_x)\Psi|^2 - |(-i\partial_y - e^*A_y)\Psi|^2]$$
$$+ \frac{\lambda_2}{2}\phi[(\partial_x\phi)^2 - (\partial_y\phi)^2]. \qquad (4)$$

Apart from the standard free energy contributions arising due to ϕ and Ψ, we have a competition term, controlled by γ (> 0), and a term that gives rise to different effective masses for Ψ

in the two directions, which is controlled by λ_1. $\mathcal{F}$ is invariant under a rotation by 90 degrees, represented by

$$x \to y, \quad y \to -x, \quad \phi \to -\phi. \tag{5}$$

We will be interested in the limit of $\Lambda \to \infty$, where Λ is the London penetration depth, so we can neglect the coupling to the electromagnetic field. At the outset, we set $\lambda_2 = 0$, since the λ_2 term is small compared to the λ_1 term in the limit where ϕ is small. It is convenient to define the coherence length of Ψ and the healing length of ϕ as

$$l_\psi = \sqrt{\frac{\kappa_\psi}{\psi_0^2}}, \quad l_\phi = \sqrt{\frac{\kappa_\phi}{\phi_0^2}}. \tag{6}$$

Taking the unit of distance to be l_ϕ, we can recast the above free energy in a more transparent form as follows:

$$
\begin{aligned}
\mathcal{F} = {} & \frac{1}{2l^2}(\tilde{\nabla}\tilde{\psi}^*)(\tilde{\nabla}\tilde{\psi}) - \frac{1}{2}|\tilde{\psi}|^2 + \frac{1}{4}|\tilde{\psi}|^4 \\
& + \left(\frac{\gamma}{\gamma_s}\right)^2 \left[\frac{1}{2}(\tilde{\nabla}\tilde{\phi})^2 - \frac{1}{2}\tilde{\phi}^2 + \frac{1}{4}\tilde{\phi}^4\right] + \frac{\gamma^2}{2\gamma_s}|\tilde{\psi}|^2\tilde{\phi}^2 \\
& + \lambda\tilde{\phi}[(\partial_{\tilde{x}}\tilde{\psi}^*)(\partial_{\tilde{x}}\tilde{\psi}) - (\partial_{\tilde{y}}\tilde{\psi}^*)(\partial_{\tilde{y}}\tilde{\psi})], \tag{7}
\end{aligned}
$$

where $l = l_\phi/l_\psi$, $\gamma_s = \gamma\psi_0^2/\phi_0^2$, $\lambda = \lambda_1/2l_\phi^2\psi_0^2$, $\tilde{x}, \tilde{y} = x/l_\phi, y/l_\phi$, $\tilde{\psi} = \Psi/\psi_0$, and $\tilde{\phi} = \phi/\phi_0$. From now on, we will drop the tilde symbols.

For $\lambda \neq 0$, a short-distance cutoff has to be imposed on Eq. (7). Otherwise, the system is unstable toward developing modulations of ψ with sufficiently short wavelength. We discuss the instability in Appendix A. In practice, we will mostly ignore this issue, assuming that there is a short-distance cutoff (which is provided by the finite grid used in our numerical calculations).

Before we begin our analysis, let us comment about the choice of parametrization in this problem. We think of this problem in terms of a fixed $\gamma \leqslant 1$. Then, on choosing a particular ratio of the length scales of ϕ and ψ, we still have one degree of freedom left in terms of the masses or the stiffnesses of the two order parameters, which is fixed by tuning γ_s.

If we assume that $\gamma_s > 1$, then the uniform ground state is given by $\psi = 1$ and $\phi = 0$. This also constrains ϕ to be localized around the vortex cores by making the mass term for ϕ positive deep inside the superconducting region. If we further assume that the nematic order is small, such that $\frac{\gamma}{2}\phi^2 \ll \psi_0^2$, then we can essentially ignore the feedback of ϕ on ψ. Therefore, we will first find the full profile of $\psi = \Psi_0$, the isolated vortex solution, in the absence of the nematic order and use that to find the form of the nematic order. Then Ψ_0 satisfies the following asymptotic relations:

$$\Psi_0(\rho) \approx \left[1 - \frac{1}{2}\left(\frac{1}{l\rho}\right)^2\right]e^{i\theta}, \quad \rho \gg l^{-1}, \tag{8}$$

$$\Psi_0(\rho) \sim Cl\rho e^{i\theta}, \quad \rho \ll l^{-1}, \tag{9}$$

where $\rho = r/l_\phi$, r being the radius in the original coordinate system, and C is a dimensionless constant. In general, it is difficult to find the solution of the full LG equation for Ψ_0 for all ρ analytically. Therefore, we obtain the vortex solution $\Psi_0 = f(l\rho)e^{i\theta}$ for all ρ by minimizing the functional in Eq. (7) numerically in the absence of ϕ.

The numerical solution conforms to the two asymptotic expressions above. It is interesting to note that Ψ_0 does not recover from the vortex core to its bulk value exponentially but rather as a power law.[16,17] The behavior of $\phi(\rho)$ in the vicinity of a vortex with $\lambda = 0$ was studied by Ref. 16.

III. PHASE DIAGRAM

We will now describe the mean-field phase diagram of a single vortex in the presence of a competing nematic order. There are three possible phases: in phase I, $\phi = 0$ everywhere; in phase II, ϕ vanishes at large distance from the vortex core but becomes nonzero near the vortex core due to the suppression of the competing ψ field to zero at the core; and in phase III, $\phi \neq 0$ even far away from the core. A nonzero solution for ϕ is favored whenever the smallest eigenvalue ϵ of the following eigenvalue problem:[16]

$$\{-\nabla_\rho^2 - 1 + \gamma_s[f(l\rho)]^2\}\phi(x) = \epsilon\phi(x), \tag{10}$$

satisfies $\epsilon < 0$. In order to find the phase diagram, we solve this eigenvalue problem numerically on a discrete grid. The boundary between phases I and II is the locus of points at which the smallest eigenvalue satisfies $\epsilon = 0$. For $\gamma_s < 1$, ϕ becomes long ranged, corresponding to phase III. The resulting phase diagram is shown in Fig. 1. This phase diagram is strictly valid as long as $\gamma_s > \gamma$. If this is not the case, then the state with uniform nematic background and no superconductivity is energetically favorable over any other state.

The physics behind the phase diagram can be understood as follows. When $l_\phi \gg l_\psi$ we are forcing the nematic order to coexist with superconductivity in a large region. This is unfavorable energetically due to the competition term $\gamma\phi^2|\Psi|^2$. Therefore, when $\gamma_s > 1$, there is no $\phi \neq 0$ solution. If $\gamma_s < 1$, ϕ becomes nonzero, even far away from the vortex
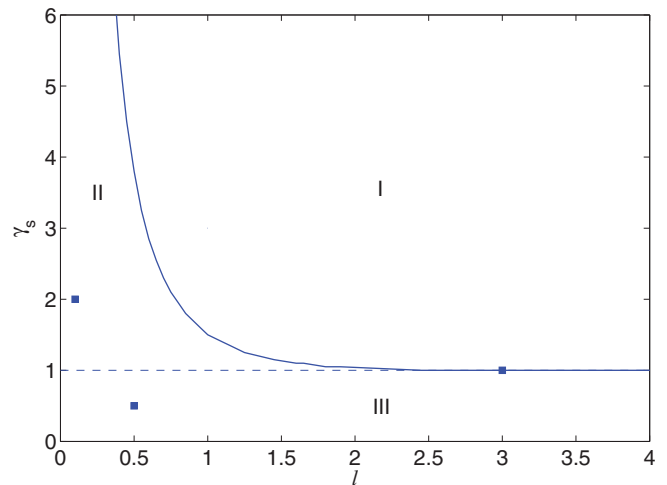

FIG. 1. (Color online) The phase diagram in the (γ_s, l) plane, obtained by solving Eq. (10) numerically on a grid with $n = 100$ and $\Delta x = 1$. The regions with qualitatively different solutions for ϕ are marked. Phase I has no nematic order with $\phi = 0$ everywhere, phase II has nematic order localized in the vortex core, and phase III has long-range nematic order away from the core. The (blue) squares correspond to points that we explore in more detail later. The dashed line $\gamma_s = 1$ represents the boundary between phases II and III.

core. In the opposite limit of $l_\phi \ll l_\psi$, the nematic order exists deep within the superconducting vortex. Since there is very little overlap between the two order parameters, the system can afford to have a higher value of critical γ_s below which there is a nontrivial nematic order. This explains the increasing trend of the critical γ_s for decreasing l.

In the $l_\phi \ll l_\psi$ case, it is possible to give an analytical expression for the phase boundary between regions I and II. The equation for this curve is given by

$$\gamma_s = \frac{1}{4(Cl)^2}. \tag{11}$$

where C is the constant which appears in Eq. (9). The details of this computation are discussed in Sec. V A.

We are now in a position to include the effect of the anisotropy and investigate the structure of the vortex cores in different regions of the phase diagram described above.

IV. VORTEX PROFILE IN THE DIFFERENT REGIMES

We now turn to discuss the characteristics of the vortex profile in the different regimes shown in Fig. 1. To solve for the vortex profile, we minimize the free energy (7) with respect to ψ and ϕ numerically on a disk geometry. This is equivalent to solving the coupled Landau-Ginzburg

equations with Neumann boundary conditions, as we discuss in Appendix B. Many of the features found in the numerical solution can be understood analytically, as we discuss in the next section.

We can expand both ψ and ϕ in terms of the different angular-momentum channels ($\sim e^{in\theta}$). The term proportional to λ only couples angular-momentum channels that differ by 2 units of angular momentum in ψ. Therefore, in the presence of ϕ, the bare vortex solution ($\sim e^{i\theta}$) gives rise to components of the form $e^{3i\theta}$, $e^{-i\theta}$, and so on. Similarly, the feedback of the superconducting order on ϕ gives rise to the generation of the even harmonics, i.e., Φ_0 gives rise to terms proportional to $e^{2i\theta}$ and $e^{-2i\theta}$. It is also possible to have a solution with only the even harmonics of ψ, in which case, the vortex is absent. These two solutions do not mix with each other and, therefore, we shall focus on the solution in the presence of the vortex.

In light of this, we expand the order parameters as

$$\psi(\rho,\theta) = \sum_n \Psi_n(\rho)e^{i(2n+1)\theta},$$
$$\phi(\rho,\theta) = \sum_n \Phi_n(\rho)e^{i2n\theta}, \quad n \in \text{integers}. \tag{12}$$

In terms of the expansions in Eq. (12), the free energy density can be written as

$$
\begin{aligned}
F_\rho = \int d\theta \mathcal{F} &= \sum_n \frac{1}{2l^2}\left[\left(\frac{\partial \Psi_n}{\partial \rho}\right)^2 + \frac{(2n+1)^2 \Psi_n^2}{\rho^2}\right] - \frac{\Psi_n^2}{2} + \frac{1}{4}\sum_{n,p,q}\Psi_n\Psi_{n+p-q}\Psi_p\Psi_q \\
&+ \left(\frac{\gamma}{\gamma_s}\right)^2\left\{\frac{1}{2}\left[\sum_n\left(\frac{\partial \Phi_n}{\partial \rho}\right)^2 + \frac{(2n)^2}{\rho^2}\Phi_n^2 - \Phi_n^2\right] + \frac{1}{4}\sum_{n,p,q}\Phi_n\Phi_{n+p-q}\Phi_p\Phi_q\right\} \\
&+ \frac{\lambda}{2}\sum_{m,p}\phi_p\left(\left[\frac{\partial \Psi_m}{\partial \rho} - (2m+1)\frac{\Psi_m}{\rho}\right]\left\{\frac{\partial \Psi_{m+p+1}}{\partial \rho} + [2(m+p+1)+1]\frac{\Psi_{m+p+1}}{\rho}\right\}\right. \\
&+ \left.\left[\frac{\partial \Psi_m}{\partial \rho} + (2m+1)\frac{\Psi_m}{\rho}\right]\left\{\frac{\partial \Psi_{m+p-1}}{\partial \rho} - [2(m+p-1)+1]\frac{\Psi_{m+p-1}}{\rho}\right\}\right) + \frac{\gamma^2}{2\gamma_s}\sum_{n,p,q}\Psi_n\Psi_{n+p-q}\Phi_p\Phi_q, \tag{13}
\end{aligned}
$$

and we are interested in minimizing $\int \rho d\rho F_\rho$. We shall minimize the above free energy for a given system size and for only a fixed number of harmonics at a time. We have kept n harmonics for ψ and ϕ, where for any given n (odd) we take all the harmonics Ψ_{-i} to Ψ_i, $i = (n-1)/2$, and similarly for ϕ. We have tried $n = 3,5$ and found no substantial qualitative change in the results that we shall quote here, indicating that the results converge even with only three harmonics. We consider a system on a disk of radius $\rho = 100$.

Below, we describe the results in regions II and III of the phase diagram and on the critical line dividing them (in region I, where there is no nematic order, we get the regular circularly symmetric vortex). The specific values of γ_s, l which were used are marked by blue squares in the phase diagram in Fig. 1.

A. Region II

In this region, we expect to obtain a solution with a nonzero uniform $|\psi|$ away from the vortex core and a nonzero ϕ localized near the vortex core, decaying exponentially away from the core (given that $\gamma < \gamma_s$ and $\gamma_s > 1$). The contour plot for $|\psi|^2$ is shown in Fig. 2. The parameters used here are $\gamma_s = 2.0$, $l = 0.1$, $\gamma = 1.0$, $\lambda = 20.0$.

As can be seen in the figure, the core has an elliptical shape because of the interaction with the nematic order that coexists with superconductivity in the core region. As we go away from the core, the contours of equal $|\psi|^2$ become more and more isotropic, due to the rapid decay of the nematic order away from the core.
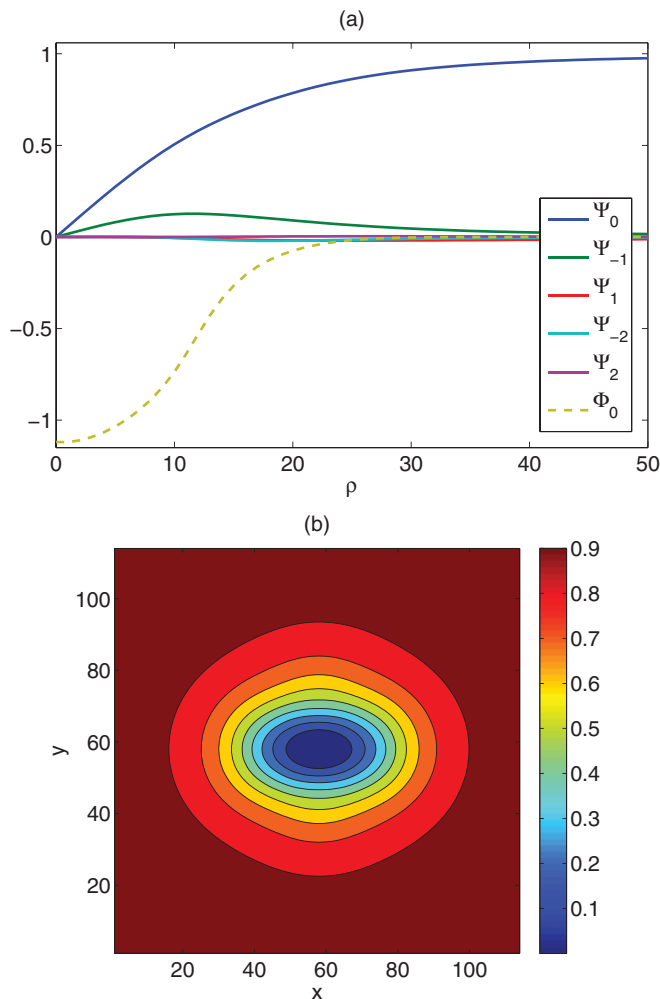
FIG. 2. (Color online) Nematic order in phase II. The profiles for the different order parameters for $\gamma_s = 2.0$, $l = 0.1$, $\gamma = 1.0$, $\lambda = 20.0$ for a system size of 100 ($N = 100$, $\Delta x = 1$). (a) Harmonics of ψ (solid lines) and Φ_0 (dashed line) (b) Contour plot of $|\psi|^2$. The superconducting coherence length l_ψ is 10, in units of l_ϕ.

B. Region III

This region in the phase diagram corresponds to the case where there is a uniform nematic background coexisting with superconductivity, even away from the vortex core. In this regime, as we move away from the core, ϕ goes to a constant and ψ remains anisotropic. In Fig. 3, the harmonics Ψ_1 and Ψ_{-1} are almost constant for large ρ. Moreover, $\Psi_1 = -\Psi_{-1}$ for large ρ. The contour plot of $|\psi|^2$ reveals a large anisotropic "halo" around the core, with a nonelliptical shape.

Far away from the core, where ϕ is constant, the Landau-Ginzburg equations can be solved analytically, showing that the anisotropy in $|\psi|^2$ decays as a power law in this case. We discuss this solution in the next section.

C. Critical case

Finally, we discuss the critical line separating regions II and III in Fig. 1, in which the ϕ field is critical far away from the core. Naively, one would expect ϕ to go as $1/\rho$
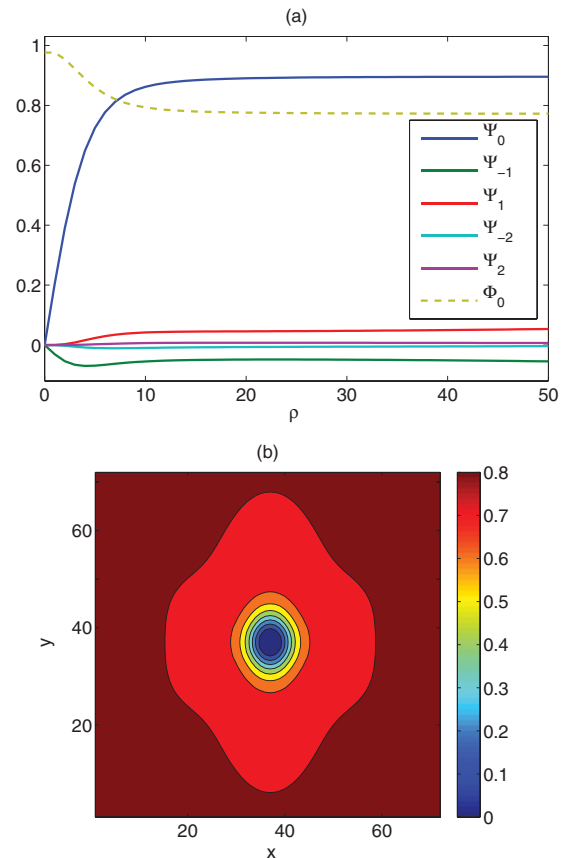

FIG. 3. (Color online) Nematic order in phase III. The profiles for the different order parameters for $\gamma_s = 0.5$, $l = 0.5$, $\gamma = 0.4$, $\lambda = 0.5$ for a system size of 100 ($N = 100$, $\Delta x = 1$). (a) Harmonics of ψ (solid lines) and Φ_0 (dashed line). (b) Contour plot of $|\psi|^2$. The superconducting coherence length is 2, in units of l_ϕ.

asymptotically in this regime. However, depending on the details of the solution at small ρ, there may be an intermediate regime in which $\phi \sim \ln \rho$, eventually crossing over to $1/\rho$ at a larger distance. This feature is discussed in more detail in the next section. Figure 4(a) shows ψ and ϕ in the critical regime, with $\gamma_s = 1.0$, $l = 3.0$, $\gamma = 0.9$, and $\lambda = 0.07$. Indeed, we observe that ϕ decays slowly away from the core. $\Psi_{\pm 1}$ also have long tails. The contour plot for $|\psi|^2$ shares features that are similar to the behavior in region III, namely a long-range, nonelliptical anisotropic halo. It is shown in Fig. 4(b).

In the next section, we analyze the asymptotic behavior of the solution in the critical case, showing that the anisotropic component of $|\psi|^2$ falls off as $\sim (\lambda \ln \rho / \rho^2) \cos(2\theta)$ at intermediate ρ, crossing over to $\sim (\lambda / \rho^3) \cos(2\theta)$ at sufficiently large ρ.

V. ANALYTICAL TREATMENT

In this section, we propose various analytical arguments to explain the different features that were observed above by carrying out the minimization numerically. In subsection V A, we discuss the solution for the nematic order in the presence of superconductivity. Then in subsection V B, we analyze
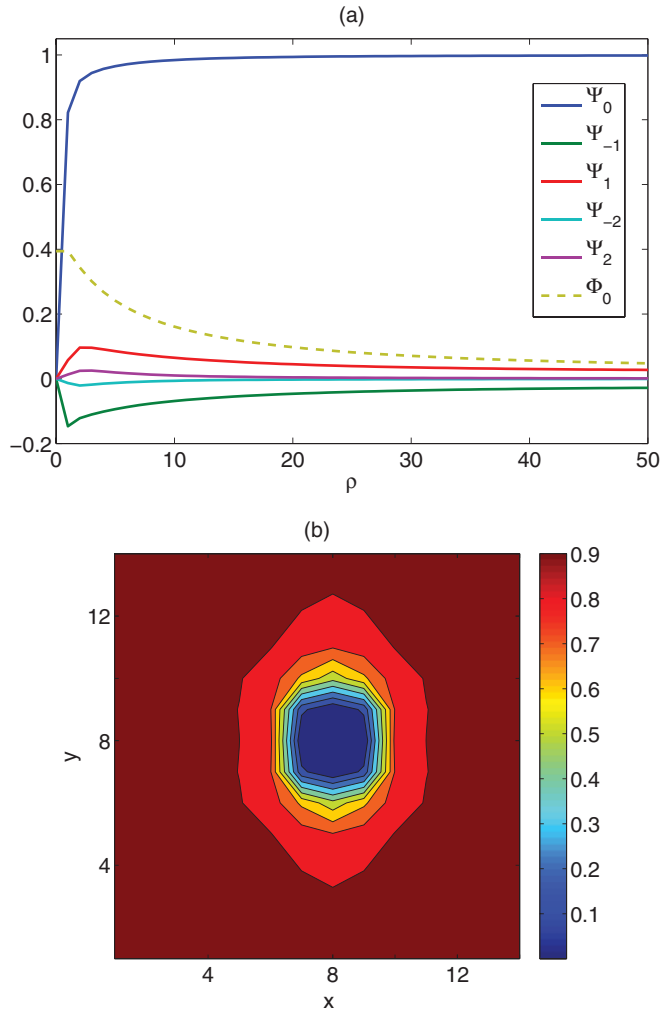
FIG. 4. (Color online) Nematic order at the critical point between phase III and phase I. The profiles for the different order parameters for $\gamma_s = 1.0$, $l = 3.0$, $\gamma = 0.9$, $\lambda = 0.07$ for a system size of 100 ($N = 100$, $\Delta x = 1$). (a) Harmonics of ψ (solid lines) and Φ_0 (dashed line). (b) Contour plot of $|\psi|^2$. The superconducting coherence length is $1/3$, in units of l_ϕ.

region III of the phase diagram (Fig. 1). Finally, in subsection V C, we study the linearized GL equations in order to explain some of the other interesting features that were observed earlier.

A. Phases of the nematic order

Here we will briefly review the solution for ϕ and supplement it with some further details. The LG equation for $\phi(\rho)$, assuming that $\lambda = 0$, is given by

$$\left\{ -\nabla_\rho^2 - 1 + \gamma_s[f(l\rho)]^2 + \phi^2 \right\}\phi = 0. \qquad (14)$$

We shall now be interested in solving the linearized version of the above equation, which is justified for $\gamma_s > 1$. For $\rho \ll l^{-1}$, this becomes equivalent to solving the problem

$$\left[-\nabla_\rho^2 - 1 + \gamma_s(Cl\rho)^2 \right]\phi = 0. \qquad (15)$$
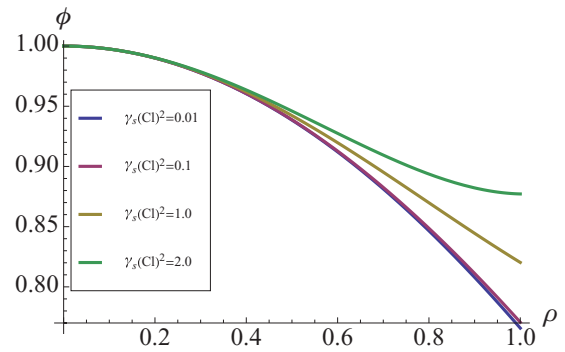

FIG. 5. (Color online) The profiles of ϕ as a function of ρ for different values of $\gamma_s C^2 l^2$ over a distance of one correlation length of ϕ, l_ϕ.

This is identical to solving the Schrödinger equation for the 2D quantum harmonic oscillator. We know that $\phi'(\rho = 0) = 0$. The solution for this equation is given by

$$\phi(\rho) = e^{-\sqrt{\gamma_s C^2 l^2}\rho^2/2}\frac{\mathcal{L}_a(\sqrt{\gamma_s C^2 l^2}\rho^2)}{\mathcal{L}_a(0)}, \quad a = \frac{1 - 2\sqrt{\gamma_s C^2 l^2}}{4\sqrt{\gamma_s C^2 l^2}}, \qquad (16)$$

where $\mathcal{L}_n(x)$ are the Laguerre polynomials. The profiles of $\phi(\rho)$ for a few different values of $\gamma_s C^2 l^2$ are shown in Fig. 5.

At this point, we can also describe how we obtained the equation for the phase boundary between regions I and II in the phase diagram (Fig. 1). In this case, ϕ is nonzero only very close to the center of the core. We can, therefore, expand ψ around $\rho = 0$ and keep only the leading-order term [Eq. (9)]. Equation (15) can be rewritten as

$$\left[-\frac{\nabla_\rho^2}{2} + \frac{\gamma_s C^2 l^2}{2}\rho^2 \right]\phi = \left(\frac{1}{2} + \epsilon \right)\phi. \qquad (17)$$

Nontrivial solutions exist for $\epsilon \leqslant 0$. The above equation is the Schrödinger equation for a quantum harmonic oscillator in two dimensions with $m = 1$, $\omega^2 = \gamma_s(Cl)^2$. Then the smallest eigenvalue which corresponds to the zero-point energy of the oscillator leads to the following equation for the curve

$$\gamma_s = \frac{1}{4(Cl)^2} \qquad (18)$$

in the limit of small l.

On the other hand, for $\rho \gg l^{-1}$, we have to solve

$$\left\{ -\nabla_\rho^2 - 1 + \gamma_s\left[1 - \frac{1}{(\rho l)^2} \right] \right\}\phi = 0, \qquad (19)$$

from which we see that $\phi(\rho) \sim \rho^{-1/2}\exp(-\sqrt{\gamma_s - 1}\rho)$. However, there is a *fine-tuned* point at $\gamma_s = 1$, at which the field ϕ is critical far away from the vortex core. The full equation for ϕ becomes

$$\left[-\nabla_\rho^2 - \frac{1}{(\rho l)^2} + \phi^2 \right]\phi = 0, \qquad (20)$$

$\phi(\rho) = \sqrt{1 + l^2}/(l\rho)$. Note that the $1/\rho$ solution can be obtained only for specific boundary conditions. For generic

boundary conditions, with $\phi \to 0$ as $\rho \to \infty$, the solution is, nevertheless, asymptotic to $\sqrt{1+l^2}/(l\rho)$ at large ρ. If $\phi(1) \ll 1$, for instance, then $\phi(\rho) \sim A \ln(\rho_0/\rho)$ at intermediate values of ρ, where A and ρ_0 are constants. $\phi(\rho)$ crosses over to $\phi(\rho) \sim 1/\rho$ at radii of the order of $\rho^\star \sim 1/A$ (see Appendix C). This behavior reflects itself in the asymptotic decay of the anisotropy of the field ψ away from the vortex core, as we discussed in Sec. IV.

B. Coexistence of superconductivity and nematic order

In this subsection, we are interested in analyzing region III of the phase diagram, in which superconductivity and nematicity coexist even far away from the core. Let us assume, for simplicity, that far away from the core ϕ can be replaced by a constant. The effect of a constant ϕ is to render the effective masses in the two directions different. Therefore, if we rescale the coordinates as

$$x' = \frac{x}{\sqrt{1+\alpha}}, \quad y' = \frac{y}{\sqrt{1-\alpha}}, \quad (21)$$

where $\alpha = 2\lambda\phi l^2$, then this problem now becomes identical to the isotropic problem we had solved in the beginning of Sec. II. The solution for Ψ_0 can then be written in terms of the new coordinates as

$$\Psi_0 = \frac{f(r')}{r'}(x' + iy'),$$

$$f(r') = c\left(1 - \frac{1}{2l^2c^2r'^2}\right), \quad c = \sqrt{1 - \frac{\gamma^2\phi^2}{\gamma_s}}. \quad (22)$$

Note that due to the presence of the background nematic order, Ψ_0 does not tend to 1 asymptotically. We now go back to our original coordinate system x,y by

expanding the above result to linear order in α. We then get

$$\psi = c\left(1 - \frac{1}{2l^2c^2r^2}\right)e^{i\theta} - \frac{\alpha c}{4}\left(1 + \frac{1}{2l^2c^2r^2}\right)e^{-i\theta}$$
$$+ \frac{\alpha c}{4}\left(1 - \frac{3}{2l^2c^2r^2}\right)e^{3i\theta}. \quad (23)$$

In the above expression, the first bracket corresponds to Ψ_0, the second bracket corresponds to Ψ_{-1}, and the last one represents Ψ_1. It is interesting to observe that, asymptotically, Ψ_1 and $-\Psi_{-1}$ approach the same constant value. We observe this feature in Fig. 3(a). However, the harmonics do not recover to their asymptotic value as a power law, which is a result of the boundary conditions that were imposed while minimizing the free energy in the disk geometry (see Appendix B).

From Eq. (23), we can evaluate the form of $|\psi|^2$ and find that

$$|\psi|^2 = c^2\left(1 - \frac{1}{l^2c^2r^2}\right) - \frac{\alpha}{l^2r^2}\cos(2\theta) + O(\alpha^2). \quad (24)$$

Therefore, asymptotically, $|\psi|^2$ is isotropic and the anisotropy decays as $\sim\alpha\cos(2\theta)/r^2$.

C. Linearized GL analysis

In this section, we shall carry out an analysis of the linearized LG equations to give an analytical explanation for some of the features that we have observed by carrying out the full minimization. For the sake of simplicity, let us ignore the feedback on ϕ resulting in the generation of the higher harmonics and assume that ϕ is isotropic [i.e., $\phi(\rho,\theta) = \phi(\rho)$]. The linearized LG equations for the harmonics of ψ can then be written as

$$\frac{1}{l^2}\left[\partial_\rho^2 + \frac{\partial_\rho}{\rho} - \frac{(2n+1)^2}{\rho^2}\right]\Psi_n(\rho) + \left(1 - \frac{\gamma^2}{\gamma_s}\phi^2\right)\Psi_n(\rho) - 2\Psi_0^2(\rho)\Psi_n(\rho) - \Psi_0^2(\rho)\Psi_{-n}(\rho)$$
$$= -\lambda\phi(\rho)\left\{\left[\partial_\rho^2 - (4n-1)\frac{\partial_\rho}{\rho} + \frac{(4n^2-1)}{\rho^2}\right]\Psi_{n-1}(\rho) + \left[\partial_\rho^2 + (4n+5)\frac{\partial_\rho}{\rho} + \frac{(2n+3)(2n+1)}{\rho^2}\right]\Psi_{n+1}(\rho)\right\}$$
$$+ \lambda\partial_\rho\phi(\rho)\left[\left(\partial_\rho - \frac{2n-1}{\rho}\right)\Psi_{n-1}(\rho) + \left(\partial_\rho + \frac{2n+3}{\rho}\right)\Psi_{n+1}(\rho)\right]. \quad (25)$$

There are some features of the problem that cannot be deduced from a study of the linearized version of the problem, which include the overall scale and sign of Φ and the signs of the different harmonics of ψ.

In the limit of $\rho \ll l^{-1}$, i.e., inside the vortex core, at leading order $\Psi_n(\rho) \sim \rho^a$, where $a = |2n+1|$. This is a necessary condition for the harmonics to be well behaved in the limit of $\rho \to 0$.

On the other hand, in the limit of $\rho \gg l^{-1}$, i.e., deep inside the superconducting region, the homogenous solution for the above equation gives exponentially damped solutions for all the $\Psi_{n\neq0}$, i.e., the anisotropy is short ranged. Moreover,

the source term, which is proportional to $\lambda\phi$ and is itself exponentially damped (region II), is also not strong enough to give rise to any long-ranged solution.

However, when ϕ is critical (i.e., $\gamma_s = 1$), the source term leads to the presence of long tails in the harmonics. In the regime where ϕ falls off logarithmically while Ψ_0 is a constant, at leading order $\Psi_{\pm1}$ just follow ϕ, i.e., they also fall off logarithmically (with prefactors of equal magnitude but opposite sign) and have a correction of the form $\ln\rho/\rho^2$. On the other hand, when ϕ crosses over to the power-law form, at leading order $\Psi_{\pm1}$ also fall off as $\pm1/\rho$ with a correction of order $1/\rho^3$.

VI. CONCLUSION

We have studied the interplay between nematic order and superconductivity in the presence of a vortex. If the nematic order coexists with superconductivity in the vicinity of a vortex core, the coupling between the two order parameters leads to an elongated shape of the core. We discuss two distinct scenarios: In one the nematic order coexists with superconductivity everywhere (i.e., even far away from the vortex core), whereas in the other the competition between the two order parameters suppresses the nematic order in the bulk, and nematicity exists only close to the core where the superconducting order parameter is diminished. Both scenarios lead to an anisotropic core. However, we show that they can, in principle, be distinguished by the way the anisotropy of the superconducting gap decays away from the core. If the nematicity exists only near the core, the anisotropy in the superconducting gap decays exponentially; if it exists throughout the sample, we expect the gap anisotropy to decay as $1/r^2$, where r is the distance from the core. Moreover, there are qualitative differences in the shape of the core in the two cases. In the former case, in which only the core region is nematic, the contours of equal gap tend to be more or less elliptical. In the latter case, the contours of equal gap tend to develop nonelliptical shapes with a four-petal pattern. Therefore, analyzing the gap profiles measured by STM around a vortex could reveal the nature of the nematic ordering, whether it is localized at the vortex core or coexists with superconductivity in the bulk.

So far, we have discussed the structure of an isolated vortex at the mean-field level. However, if the nematic ordering is favored only within a vortex core, an isolated vortex cannot have static nematic order, since either thermal or quantum fluctuations would destroy such order. Static nematic order is possible only when the density of vortices is finite. The coupling between the nematic halos of different vortices scales as $J_{\text{eff}} \sim \exp[-d/(\sqrt{1-\gamma_s}l_\phi)]$, where $d \sim 1/\sqrt{B}$ is the intervortex distance (B is the applied magnetic field). The system can be described by an effective two-dimensional transverse field Ising model with a spin-spin interaction J_{eff} and a B-independent transverse field. (Note that, unlike Ref. 16, we are considering a thin film rather than a three-dimensional system.) This model has a nematic transition at a certain critical B, which should be seen, e.g., by measuring the anisotropy of the vortex cores as a function of B. If an external rotational symmetry breaking field exists, as is presumably the case in FeSe due to the small orthorhombic lattice distortion,[15] the electronic nematic transition is smoothed out. However, one still expects a sharp crossover as a function of magnetic field if the orthorhombic distortion is sufficiently weak.

The microscopic origin of the anisotropic vortex cores observed in FeSe[14] remains to be understood. It is likely that it originates from electronic nematicity rather than from the lattice distortion, since the experimentally reported orthorhombic distortion seems too small to produce such a large effect. The electronic nematic order could have an orbital character.[11,18–20] Alternatively, it could arise from a field-induced magnetic ordering[21] at a wave vector $(\pi,0)$ or $(0,\pi)$ in the one iron unit cell, which is necessarily accompanied by a nematic component (similar to the ordering in the iron arsenides).

Although static ordering of this type has not been observed in the iron selenides,[22] it remains to be seen if they develop a static ordering in the presence of an applied magnetic field. Neutron scattering experiments revealed a magnetic resonance at this wave vector in the superconducting state of FeTeSe.[23] Moreover, ordering at such wave vectors nearly nests the electron and hole pockets, and, therefore, it is expected to couple strongly to superconductivity, explaining why the resulting anisotropy of the vortex cores is so large.

Note added. After this work was submitted for publication, another manuscript[24] that studied the experimental features observed in FeSe[14] came to our attention. In this paper, the authors study the effect of orbital ordering on the vortex structure in a two-band model by solving the Bogoliubov-de Gennes equations. This study is complementary to our phenomenological Ginzburg-Landau approach.

APPENDIX A : INSTABILITIES OF THE FREE ENERGY

An interesting feature associated with the LG functional introduced in Sec. II is that there is an instability to a state with modulated ψ. This arises due to a competition between two terms in the free energy, namely the ϕ and ϕ^2 terms. Let us suppose that ϕ does not vary spatially and $\psi = \beta e^{iqx}$. Then, at leading order, the contribution to the free energy from ϕ is of the form

$$\mathcal{F}_\phi = \left(\frac{\gamma^2\beta^2}{2\gamma_s} - \frac{\gamma^2}{2\gamma_s^2} \right)\phi^2 + \lambda q^2\beta^2\phi. \quad (A1)$$

From the above expression, we see that for a sufficiently large λq^2, it becomes energetically favorable to gain energy from the second term by condensing a large negative value of ϕ. By extremizing the above with respect to ϕ, we obtain $\phi_m = -\lambda\beta^2 q^2/(\frac{\gamma^2\beta^2}{\gamma_s} - \frac{\gamma^2}{\gamma_s^2})$. Hence, the contribution to free energy from ϕ_m is $\propto -\beta^2\lambda^2 q^4$. This energy gain from a nonzero q always dominates over the energy cost of order q^2 for a sufficiently large q. In order to prevent this instability, we have to add a term of the form $\zeta|\nabla^2\psi|^2/2l^4$ to the free energy, which is an allowed term from the underlying symmetry of the problem. We now want to obtain some restrictions on ζ.

First, ζ should be such that it prevents the instability. This gives us a lower bound on the value of ζ. At the same time, ζ should be small enough so it should not change the physics significantly. This gives us an upper bound on the value of ζ. Therefore, we obtain

$$\frac{\lambda^2\gamma_s^2 l^4}{\gamma^2(\gamma_s - 1)} < \zeta \ll 1. \quad (A2)$$

The above expression is not valid when ϕ becomes critical, i.e., when $\gamma_s = 1, \beta = 1$. In this case, we have to compare ϕ with ϕ^4.

However, when we minimized the free energy in Sec. IV, we did not have to include the above term with a finite ζ as for a sufficiently small λ, the cutoff in q arising from the discrete lattice prevented this instability from showing up.

APPENDIX B : EFFECT OF BOUNDARY TERMS

In general, when we derive the GL equations from the free energy, there is a surface term arising from the gradient terms in the energy that can be ignored in the limit of an infinite system size. However, for a finite-sized system, the boundary term does play an important role. Let us consider only the contribution of the gradient term of the superconducting order parameter in the free energy in the absence of any nematic order. We then have

$$F_{\text{grad}} = \int d^2 r |\nabla \psi|^2, \tag{B1}$$

$$F_{\text{tot}} = F_{\text{grad}} + F_{\text{local}}, \tag{B2}$$

where F_{local} contains the usual $|\psi|^2, |\psi|^4$ terms. On varying ψ^* by $\delta\psi^*$ in F_{tot}, we obtain, for a finite system (up to other variations due to F_{local} denoted by . . .),

$$-\int d^2 r \delta\psi^* \nabla^2 \psi + \int_{\text{surface}} \delta\psi^* (\nabla\psi)\hat{n} ds + \cdots = 0, \tag{B3}$$

where $\hat{n} ds$ is the area element, normal to the boundary. When we solve for ψ in the interior of the region, only the first term contributes and the boundary term can be ignored. However, when we solve for ψ on the boundary, only the surface term plays a role, since it can be thought of as appearing with an infinite weight of the form $\int dr \delta(r - R)$, where R is the radius of the disk on which we are minimizing the free energy and $\delta(\cdots)$ is the Dirac δ function. Therefore, in order to solve for ψ, we have to solve for $-\nabla^2 \psi + \cdots = 0$ in the interior of the region subject to the boundary condition $\nabla\psi\hat{n}|_{r=R} = 0$ (Neumann boundary conditions).

Now, in the presence of a constant nematic background (ϕ_0), the gradient term in the free energy is

$$F_{\text{grad}} = \int dx dy [(1 + \alpha)|\partial_x \psi|^2 + (1 - \alpha)|\partial_y \psi|^2], \tag{B4}$$

where $\alpha = 2\lambda\phi_0 l^2$. As we did earlier, on carrying out the variation over ψ^* this amounts to solving for $-(1 + \alpha)\partial_x^2 \psi - (1 - \alpha)\partial_y^2 \psi + \cdots = 0$ subject to the boundary condition, $\tilde{D}\psi\hat{n} = 0$, where

$$\tilde{D}\psi = [(1 + \alpha)\partial_x\psi, (1 - \alpha)\partial_y\psi], \quad \hat{n} = (\cos\theta, \sin\theta). \tag{B5}$$

In polar coordinates, this condition can be written as

$$\partial_r \psi + \alpha \left(\cos 2\theta \partial_r \psi - \frac{\sin 2\theta}{r} \partial_\theta \psi \right) = 0. \tag{B6}$$

These boundary conditions mean, in particular, that the current perpendicular to the boundary is zero. In our numerical calculations, we have used a disk geometry; therefore, the boundaries are found to have a significant effect whenever we are considering a noncircularly symmetric solution, in particular, in the regime where the nematic order is nonzero even far away from the core. We circumvent this problem, however, by taking a sufficiently large system and considering
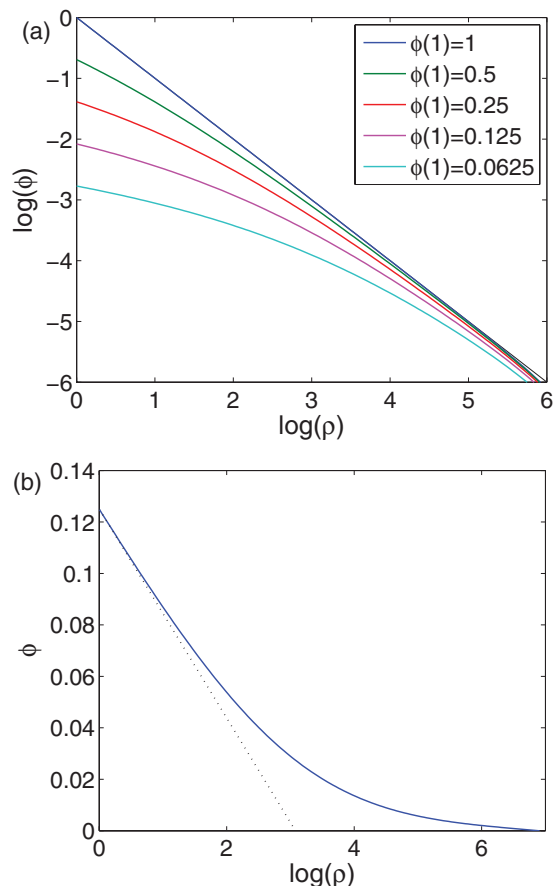

FIG. 6. (Color online) Numerical solutions of Eq. (C1). (a) Solutions with boundary conditions $\phi(1000) = 0$ and with various values of $\phi(1)$ on a log-log scale. (b) Solution with boundary condition $\phi(1) = 0.125$, $\phi(1000) = 0$, on a semilog scale. The dashed line is a fit to the form $A + B \log(\rho)$ for small ρ.

the solution only close to the vortex core, where the boundary effects are small.

APPENDIX C : ASYMPTOTICS OF ϕ IN THE CRITICAL CASE

In this appendix, we analyze the asymptotics of the field ϕ far away from the vortex core in the case $\gamma_s = 1$, in which the nematic order is critical. In this case, and for $\rho \gg 1$, the Landau-Ginzburg equation for ϕ [Eq. (14)] becomes

$$\left[-\nabla_\rho^2 + \phi^2 \right]\phi = 0. \tag{C1}$$

This nonlinear equation admits the solution $\phi(\rho) = 1/\rho$.[16] This solution is valid, however, for specific initial conditions, e.g., $\phi(1) = 1$, $\phi'(1) = -1$. Physically, the initial conditions for Eq. (C1) are determined by the details of the vortex profile at short distances, determined by Eq. (14). Nevertheless, one can make some general statements about the asymptotic behavior of the solution. If, for some arbitrary ρ_0 such that $\rho_0 \gg 1/l$ (far from the core), ϕ satisfies $\phi(\rho_0) \ll 1/\rho_0$, then it is justified to neglect the ϕ^2 term in Eq. (C1). The solution close to ρ_0 then behaves as $\phi(\rho) \approx A - B \ln(\rho/\rho_0)$, where A, B are determined by the initial conditions. This can be valid, however, only up to a point ρ_* at which $\phi(\rho_*) \approx 1/\rho_*$, i.e.,

at distances which are much smaller than the length scale set by the initial condition of Eq. (C1). At longer distances, we expect a crossover to $\phi(\rho) \approx 1/\rho$.

In Fig. 6, we present a numerical solution of Eq. (C1) with boundary conditions $\phi(1000) = 0$ and various values for $\phi(1)$. When $\phi(1) = 1$, we get $\phi(\rho) \approx 1/\rho$ (where the deviations are due to the boundary condition at $\rho = 1000$). For smaller $\phi(1)$, there is an intermediate region where ϕ does not follow a power law, eventually crossing over to $1/\rho$ at larger ρ. $\phi(\rho)$ is approximately logarithmic in the intermediate region, as shown in Fig. 6(b).

Physically, we expect that $\phi < 1$ (since $\phi = 1$ corresponds to the equilibrium value of ϕ in the absence of superconductivity). Therefore, there is an intermediate logarithmic region, which becomes parametrically large in the limit of small ϕ.

---

[1] Y. Ando, K. Segawa, S. Komiya, and A. N. Lavrov, Phys. Rev. Lett. **88**, 137005 (2002).

[2] V. Hinkov, D. Haug, B. Fauqué, P. Bourges, Y. Sidis, A. Ivanov, C. Bernhard, C. T. Lin, and B. Keimer, Science **319**, 597 (2008).

[3] Y. Kohsaka et al., Science **315**, 1380 (2007).

[4] R. Daou et al., Nature **463**, 519 (2010).

[5] M. J. Lawler et al., Nature **466**, 347 (2010).

[6] A. Mesaros, K. Fujita, H. Eisaki, S. Uchida, J. C. Davis, S. Sachdev, J. Zaanen, M. J. Lawler, and Eun-Ah Kim, Science **333**, 426 (2011).

[7] C. Fang, H. Yao, W.-F. Tsai, J.-P. Hu, and S. A. Kivelson, Phys. Rev. B **77**, 224509 (2008).

[8] C. Xu, M. Müller, and S. Sachdev, Phys. Rev. B **78**, 020501(R) (2008).

[9] T.-M. Chuang, M. P. Allan, Jinho Lee, Yang Xie, Ni Ni, S. L. Bud'ko, G. S. Boebinger, P. C. Canfield, and J. C. Davis, Science **327**, 181 (2010).

[10] J.-H. Chu, J. G. Analytis, K. De Greve, P. L. McMahon, Z. Islam, Y. Yamamoto, and I. R. Fisher, Science **329**, 824 (2010).

[11] M. Yi et al., Proc. Natl. Acad. Sci. USA **108**, 6878 (2011).

[12] M. Nakajima et al., Proc. Natl. Acad. Sci. USA **108**, 12238 (2011).

[13] J. J. Ying et al., Phys. Rev. Lett. **107**, 067001 (2011).

[14] Can-Li Song et al., Science **332**, 1410 (2011).

[15] T. M. McQueen, A. J. Williams, P. W. Stephens, J. Tao, Y. Zhu, V. Ksenofontov, F. Casper, C. Felser, and R. J. Cava, Phys. Rev. Lett. **103**, 057002 (2009).

[16] S. A. Kivelson, Dung-Hai Lee, E. Fradkin, and V. Oganesyan, Phys. Rev. B **66**, 144516 (2002).

[17] E. Demler, S. Sachdev, and Y. Zhang, Phys. Rev. Lett. **87**, 067202 (2001).

[18] R. R. P. Singh, e-print arXiv:0903.4408 (unpublished).

[19] F. Krüger, S. Kumar, J. Zaanen, and J. van den Brink, Phys. Rev. B **79**, 054504 (2009).

[20] C.-C. Chen, J. Maciejko, A. P. Sorini, B. Moritz, R. R. P. Singh, and T. P. Devereaux, Phys. Rev. B **82**, 100504(R) (2010).

[21] Similarly to the magnetic-field-induced antiferromagnetic order seen in certain cuprate superconductors. See, e.g., B. Lake et al., Nature (London) **415**, 299 (2002).

[22] S. Medvedev et al., Nat. Mater. **8**, 630 (2009).

[23] Y. Qiu et al., Phys. Rev. Lett. **103**, 067008 (2009); H. A. Mook et al., e-print arXiv:0904.2178 (unpublished).

[24] Hsiang-Hsuan Hung, Can-Li Song, Xi Chen, Xucun Ma, Qi-kun Xue, and Congjun Wu, e-print arXiv:1109.6116.